



AIAA 2004-4162

**Nonlinear Longitudinal Mode Instability in
Liquid Propellant Rocket Engine Preburners**

G. A. Flandro and J. Majdalani
Advanced Theoretical Research Center
University of Tennessee Space Institute
Tullahoma, TN 37388

J. D. Sims
NASA Marshall Space Flight Center
Huntsville, AL 35806

**40th AIAA/ASME/SAE/ASEE Joint
Propulsion Conference and Exhibit**

**11–14 July 2004
Fort Lauderdale, FL**

Nonlinear Longitudinal Mode Instability in Liquid Propellant Rocket Engine Preburners

Gary A. Flandro,* and Joseph Majdalani†
University of Tennessee Space Institute, Tullahoma, TN 37388
and
Joseph D. Sims‡
NASA Marshall Space Flight Center, Huntsville, AL 35806

Nonlinear pressure oscillations have been observed in liquid propellant rocket instability preburner devices. Unlike the familiar transverse mode instabilities that characterize primary combustion chambers, these oscillations appear as longitudinal gas motions with frequencies that are typical of the chamber axial acoustic modes. In several respects, the phenomenon is similar to longitudinal mode combustion instability appearing in low-smoke solid propellant motors. An important feature is evidence of steep-fronted wave motions with very high amplitude. Clearly, gas motions of this type threaten the mechanical integrity of associated engine components and create unacceptably high vibration levels. This paper focuses on development of the analytical tools needed to predict, diagnose, and correct instabilities of this type. For this purpose, mechanisms that lead to steep-fronted, high-amplitude pressure waves are described in detail. It is shown that such gas motions are the outcome of the natural steepening process in which initially low amplitude standing acoustic waves grow into shock-like disturbances. The energy source that promotes this behavior is a combination of unsteady combustion energy release and interactions with the quasi-steady mean chamber flow. Since shock waves characterize the gas motions, detonation-like mechanisms may well control the unsteady combustion processes. When the energy gains exceed the losses (represented mainly by nozzle and viscous damping), the waves can rapidly grow to a finite amplitude limit cycle. Analytical tools are described that allow the prediction of the limit cycle amplitude and show the dependence of this wave amplitude on the system geometry and other design parameters. This information can be used to guide corrective procedures that mitigate or eliminate the oscillations.

Nomenclature

A_p	= unsteady pressure amplitude
a_0	= mean speed of sound
e	= oscillatory energy density
\bar{E}	= time-averaged oscillatory system energy
E_m^2	= normalization constant for mode m
k_m	= wave number for axial mode m
L	= chamber length
m	= mode number
\bar{M}	= reference chamber Mach number
\mathbf{n}	= outward pointing unit normal vector
p	= oscillatory pressure

\bar{P}	= mean chamber pressure
r	= radial position
R	= chamber radius
S	= Strouhal number, k_m / \bar{M}_b
t	= time
\mathbf{u}	= oscillatory velocity vector
U_r, U_z	= mean flow velocity component
z	= axial position
α	= growth rate (dimensional, sec^{-1})
δ	= reciprocal of square root of the acoustic Reynolds number, $\sqrt{\nu / (a_0 R)}$
δ_d	= compressible viscous length, $\delta \sqrt{(\eta / \mu + \frac{4}{3})}$
ε	= wave amplitude, $A_p / (\gamma p_0)$
γ	= ratio of specific heats
η	= second coefficient of viscosity, $-\frac{2}{3}\mu$
ν	= kinematic viscosity, μ / ρ
ρ	= density
ω	= unsteady vorticity magnitude
Ω	= mean vorticity magnitude

*Boling Chair Professor of Excellence in Propulsion, Department of Mechanical, Aerospace and Biomedical Engineering. Associate Fellow AIAA

†Jack D. Whitfield Professor of High Speed Flows. Department of Mechanical, Aerospace and Biomedical Engineering. Member AIAA.

‡Engineer. Combustion Devices Group. Member AIAA.

Subscripts

- b = combustion zone
 m = specific to a given mode number

Superscripts

- * = dimensional quantity
 \sim = vortical (rotational) part
 \wedge = acoustic (irrotational) part
 $(\underline{r}), (i)$ = part of a complex variable
= mean quantity

I. Introduction

COMBUSTION instability in liquid propellant is most often associated with high frequency transverse acoustic modes. Recent experiments involving liquid rocket preburners have indicated the presence of another form of instability that is quite similar to that observed in solid propellant rockets with cylindrical combustion chambers and internal-burning propellant grains.¹⁻⁴ In these tests, oscillations are observed that are clearly associated with longitudinal acoustic waves: calculated frequencies agree closely with measured data; as usual, the first longitudinal mode is seen to constitute the predominant spectral component.

Such oscillations are not desirable from several standpoints; vibration levels measured in the tests often exceed 190 g and the oscillations are accompanied by mean pressure changes of significant amplitude. Both of these features represent a threat to the structural integrity of the system. Chamber pressure excursions are undesirable as they can alter the performance of the injection system in unpredictable ways.

An important feature of the data is the presence of a rich set of harmonics to the extent that the composite waveform appears to be steep-fronted. Again, these features are similar to those experienced in high-amplitude triggered instabilities in solid motors; it has been shown that in those systems the wave motions are traveling shock-like waves rather than standing acoustic waves.⁵⁻⁸ This solid motor problem was once dubbed *irregular burning* because the oscillations were habitually coupled with a distinct mean pressure excursion, the dreaded DC shift.^{2,9} Many early solid motor tests ended in catastrophic structural failure due to the mean pressure rise.

In this paper we bring to bear a new set of analytical tools that have evolved from many decades of struggle with the solid propellant rocket combustion instability problem. Recent work by the present authors has led to considerable progress in the development of useful predictive capability. Companion papers describe the success of these efforts.^{10,11} To be useful,

such predictive tools must go far beyond the usual "growth rate" calculations and stability maps that are commonly used. It is necessary to accommodate the nonlinear aspects of the problem in detail. The presence of steep-fronted waves and the associated mean pressure rise clearly indicate the presence of nonlinear behavior in the preburner instability problem. In order to handle this situation, the analysis must account for:

- Steep-fronted, traveling, shocked pressure waves.
- Combustion coupling including: unsteady distributed energy release, detonation wave phenomena, and interactions with the propellant injection processes.
- Surface effects including heat transfer and frictional energy losses.

Each of these elements receives due consideration in the approach to be presented here. In the process, application to prediction, diagnosis and correction of liquid engine preburner longitudinal oscillations will be demonstrated.

II. Experimental Observations

In this section, we briefly outline what has been observed in recent preburner test experience. Due to the sensitive nature of this information, actual data is not displayed. However, similar data from solid rockets tests will be described in considerable detail. The similarities between the two data sets will be quite apparent.

A. Description of Typical Preburner Geometry

A very simple burner geometry will be described consisting of an injector surface at the head-end through which liquid hydrogen and liquid oxygen are inserted into the combustion chamber. Figure 1 is a schematic of the test apparatus. The mixture is deliberately very fuel rich in the case described. In the preburner test device, a choked Laval nozzle is utilized as shown in

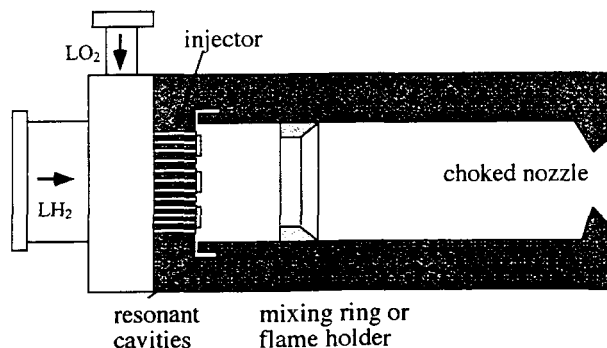


Fig. 1 Schematic of preburner test device.

the diagram. Other features sometimes employed include mixing rings or flame holders and acoustic cavities intended to suppress undesirable high-frequency tangential mode gas oscillations. The latter device, does not, unfortunately, provide significant damping for the control of longitudinal oscillations.

B. Description of Typical Preburner Tests

Tests are conducted by ramping up the fuel and oxidizer flows to an intermediate throttle level. In some experiments, it was during this mid-throttle level that high-amplitude, longitudinal mode pressure oscillations were experienced. When throttle setting was further advanced, the oscillations were suppressed.

A typical record with low frequency resolution is shown in Fig. 2(a). Pressure sensors were placed at several locations at the chamber boundaries including the injector surface and the nozzle entrance. Pressure data were also secured at points within the LOX and H₂ injectors. Figure 2(b) shows a typical steep-fronted wave form measured near the injector face; the frequency of this wave closely corresponds to the first longitudinal acoustic mode. The spectrum is illustrated in Fig. 2(c). Pressure data were also secured at points within the LOX and H₂ injectors. In general, these measurements also showed spectral characteristics,

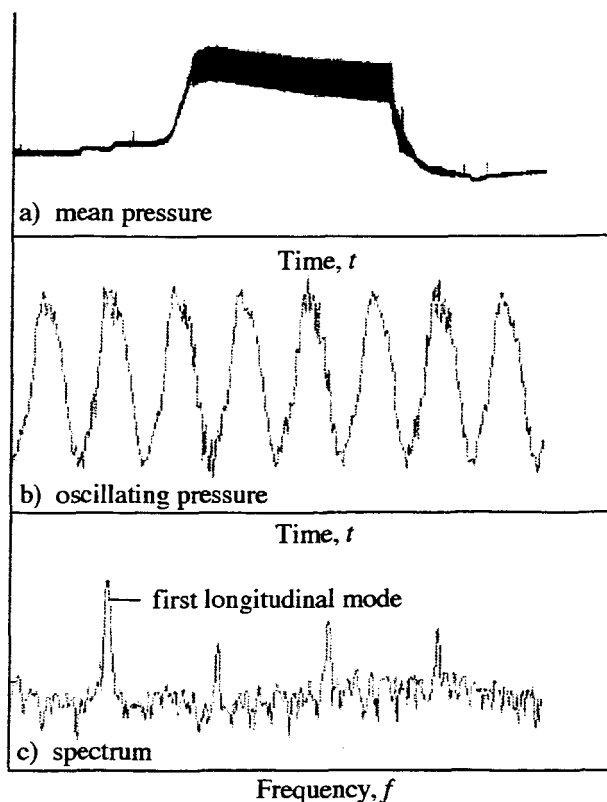


Fig. 2 Typical pressure measurements.

mean pressure shift, and oscillations that followed those measured in the main chamber. However, there were phase shifts as one would expect between the LOX and H₂ pressure fluctuations and the oscillations measured within the combustion chamber near the injector face. This set of observations play a major role in identifying the mechanisms that lead to the oscillations. These matters will be carefully examined after the basic mathematical formulation needed in interpreting the data is set forth.

III. Analysis

Classical analyses have utilized the assumption of a system of irrotational acoustic waves. Experimental data often motivates this approach since, as in the preburner case described here, observed oscillation frequencies are readily correlated with the standing acoustic modes of the chamber. However, assuming an acoustic basis for an instability theory results in the inability to accommodate correct boundary conditions (such as the no-slip condition at chamber boundaries) and the loss of important flow features such as unsteady vorticity that can have major impact on the validity of the results. It is also difficult to properly treat finite amplitude waves using an acoustic model. There is much evidence that the high-amplitude wave systems in unstable rockets are more akin to traveling shock fronts.¹²⁻¹⁵ Early efforts were made to account for steepened wave effects⁶⁻⁷, but the analytical methods applied did not lead to practical solutions. These were usually applications of the method of characteristics that did not lend themselves well to generalized computational techniques of the kind needed for a practical stability assessment algorithm.

A. Experience with Solid Propellant Motors

The well-known failure of predictive algorithms in solid rocket analysis is largely the result of neglect of key features of the unsteady flow of combustion products. In particular, one must account for effects of vorticity production and propagation and for the tendency of initially weak (essentially acoustic) waves to steepen into shock-like wave motions. When such waves interact with a combustible mixture of injectants, then the possibility of unsteady detonation waves must also be addressed. Very significant improvement in predictive capability results from inclusion of these features, which until recently were not included in either liquid or solid motor analyses.

Solid propellant rocket motor analysis as applied in the SSP (Standard Stability Prediction) computer program, implements Culick's irrotational acoustics based analyses.^{8,16-25} While the Culick approach introduces a more complete formulation than similar

algorithms in the accepted liquid rocket tool kit, it does not yield satisfactory predictive capability. This is partly the result of the assumption that the wave motions are strictly acoustic (irrotational) in nature. Recent work by the writers of the present paper focused on improving SSP (Standard Stability Prediction computer program) by inclusion of important mechanisms such as vorticity generation and shock wave interactions. Much of the recent progress in the solid motor analysis leads directly to similar improvements in handling the liquid rocket instability problem.

B. Rotational Flow Effects

Considerable progress has been made in the last decade in understanding both the precise source of the vorticity and the resulting changes in the oscillatory flow-field. Analytical,^{17,26-33} numerical,³⁴⁻³⁹ and experimental investigations⁴⁰⁻⁴³ have demonstrated that rotational flow effects play an important role in the unsteady gas motions in solid rocket motors. Much effort has been directed to constructing the required corrections to the acoustic model. This has culminated in a comprehensive picture of the unsteady motions that agrees with experimental measurements,^{17,26,27} as well as numerical simulations.²⁸

These models were used in carrying out three-dimensional system stability calculations,^{17,26} in a first attempt to account for rotational flow effects by correcting the acoustic instability algorithm. In this process one discovers the origin, and the three-dimensional form, of the classical *flow-turning* correction; related terms appear that are not accounted for in the SSP algorithm. In particular, a rotational correction term was identified that cancels the flow-turning energy loss in a full-length cylindrical grain. However, all of these results must now be questioned because they are founded on an incomplete representation of the system energy balance.

Culick's stability estimation procedure is based on calculating the exponential growth (or decay) of an irrotational acoustic wave; the results are equivalent to energy balance models used earlier by Cantrell and Hart.⁴⁴ In all of these calculations the system energy is represented by the classical Kirchhoff (acoustic) energy density. Consequently, it does not represent the *full* unsteady field, which must include both acoustic and rotational flow effects. Kinetic energy carried by the vorticity waves is thus ignored. It is then readily demonstrated that the actual average unsteady energy contained in the system at a given time is about 25% larger than the acoustic energy alone.¹⁸ Furthermore, representation of the energy sources and sinks that determine the stability characteristics of the motor

chamber must also be modified. Attempts to correct the acoustic growth rate model by retention of rotational flow source terms only,^{17,26} preclude a full representation of the effects of vorticity generation and coupling.

In liquid engines, the main role played by the rotational flow interactions is in controlling boundary conditions at the chamber walls and especially at the injector boundaries. Vorticity is created in the case of waves traveling parallel to the injection interface because such waves (tangential modes for example) represent unsteady pressure gradients across the incoming quasi-steady flow streamlines. This vorticity is propagated into the chamber mainly by convection, and it has important implications in terms of the motor stability. For the preburner oscillations with gas motions in a direction parallel to the burner axis and hence normal to the injector surface, no rotational corrections from wave interactions are necessary. However, since the flow near the flame-holder or mixing ring is highly sheared, it is possible that vortex shedding leading to an additional source of acoustic energy may be present. Clearly this is an additional rotational flow effect that has been an important element in some rocket motor instability problems.⁴⁵⁻⁴⁷ In the present case, there is some evidence that vortex shedding is present; frequencies that do not fit with the acoustic modes are sometimes present. However, there is compelling evidence that the major source of energy driving the observed oscillations comes from nonlinear interactions of a steep wave system with unsteady injection of the propellants and the resultant oscillatory release of energy in the combustion and mixing processes.

C. Nonlinear Effects

The effects of nonlinear interactions play a major role in controlling the nonlinear attributes of pressure oscillations in liquid motor combustion chambers. Thus strictly linearized models are of little value in the present situation. Of crucial importance is the modeling of the time history of the oscillations and their limiting amplitude and the critical triggering amplitudes at which an otherwise stable motor is caused to transition to violent oscillations. Pulsing of this sort can occur from random "popping" and other natural disturbances, so it is important to characterize this aspect of motor behavior. In the preburner case, there is no evidence of triggering, although pressure disturbances created during the startup process could act as a trigger mechanism.

It is well-known that shock waves are a major nonlinear attribute of axial mode oscillations in solid rockets.⁴⁻⁷ There is no question that shock-like features

characterize the gas motions described in Fig. 2. The steepening process is a natural feature of nonlinear resonant oscillations of gas columns.^{48,49} Recognition of the major role played by shock waves in combustion instability is not widespread in the present research community, although many past investigators have explored this possibility.^{6,7,50-52} Current liquid rocket engine instability prediction methods do not incorporate this important aspect of the problem.

D. Formulation of Nonlinear Stability Algorithm

In this section we briefly discuss what is needed from the theoretical standpoint to provide a useful analytical framework for combustion instability. It is necessary to accommodate the features we have identified as key elements in a correct physical representation. We must discard models based on the acoustic point of view. Nonlinear energy losses in steep wave fronts and energy flow to the wave structure from combustion must be accommodated. It is also necessary to provide a framework that can ultimately include effects of mixing, vaporization, and other two phase flow effects. These elements will be included only in outline form, but placeholders are inserted which will require later elaboration. By far the most effective method for incorporating this large array of physical/chemical interactions is by using a global nonlinear energy balance. Methods based on the usual perturbed acoustic wave equation cannot properly account for the many interactions that must be included.

E. Mathematical Strategy

Since the handling of steep fronted waves is of principal concern, it is necessary to carefully lay out a solution technique that will lead to a practical predictive algorithm. To make the mathematical problem tractable, we choose to avoid fashionable numerical strategies such as method of characteristics or a full CFD treatment of the problem. Either of these techniques would likely absorb an excess of time and resources, and in the end would fail in the problem we attempt to solve here. What is required is an approach that bridges the gap between the earlier perturbation techniques (that limit the solutions to linear gas motions near the stability boundary) and other *ad hoc* methods such as those introduced by Culick to study nonlinear features of combustion instability.^{19,53} In those works, Culick and his coworkers model the steepening process in which energy flows by a process of nonlinear mode coupling. In these calculations, one traces the flux of energy from low frequency to higher frequency spectral components.

In the problem of central interest here, we are not concerned with the steepening process, *per se*, rather we wish to understand the gas motions in their fully steepened state. Figure 3 illustrates several aspects of the problem that must be addressed; it portrays all key features of nonlinear combustion instability that appear experimentally. Furthermore, it suggests a useful way to categorize the various analytical methods by which we attempt to understand this very complicated physical

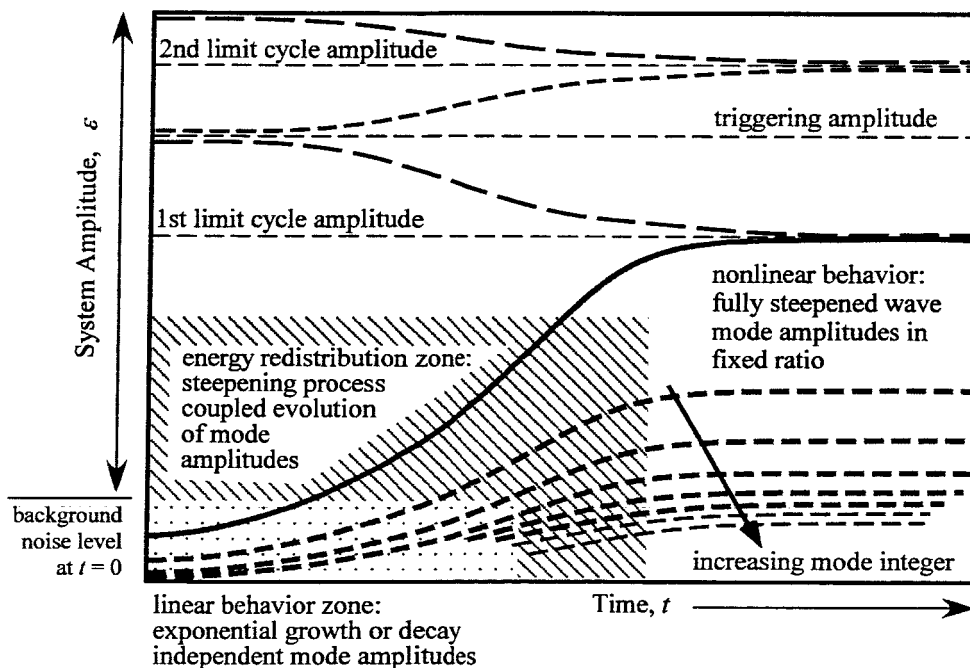


Fig. 3 Evolution of system amplitude.

problem. If the waves grow from the always present noise in the system, the motion is linear and each acoustic mode grows individually according to the balance of energy gains and losses peculiar to that operating frequency. In general, the lowest-order mode grows most rapidly because it requires less energy to excite. As the oscillations approach a finite amplitude, nonlinear effects begin to appear and there is a phase in which energy is redistributed from lower to higher modal components; it is this process that is represented in Culick's nonlinear model.

As the wave steepens, the relative amplitudes of the constituent acoustic modes reach a "frozen" or stationary condition corresponding to shock-like behavior. This is the fully nonlinear state illustrated in the figure. In pulse testing of motors, the steepening process is almost instantaneous. For example, in his solid rocket tests, Brownlee⁵ notes that when the pulse is fired, "... the injected flow disturbance traversed the length of the motor, partially reflected at the nozzle end, and became a steep-fronted shock-like wave in one cycle." Thus in modeling such effects, it is unnecessary to trace the full steepening process as Culick attempts to do. The relative wave amplitudes are readily estimated from a large database of experimental data to be described later, and these remain fixed whenever the driving mechanisms continue to supply sufficient energy to the oscillating system. Thus, it is readily established that precise knowledge of the relative amplitudes is not necessary to achieve an accurate estimate of the limit cycle and triggering amplitudes.

We must formulate a mathematical strategy that yields essential information, namely the limit amplitude reached by the system in its fully steepened state. This is the knowledge required by the engine system designer in assessing potential vibration levels, and as we will show, the severity of heat loads and force levels on fragile injector components.

The key to simplifying the nonlinear problem is to assume that the fully steepened *traveling* wave is a composite of the chamber normal modes:

$$p(r, t) = \varepsilon(t) \sum_{m=1}^{\infty} A_m(t) \psi_m(r) \quad (1)$$

where $\varepsilon(t)$ is the instantaneous amplitude. This is a proven strategy^{6,7} that conforms in all respects to all behavioral characteristics observed experimentally. These must obviously be accommodated in our solution algorithm. Before proceeding with the analysis, let us first test this model to see if it contains the necessary features.

F. Shocked Acoustic Waves

Equation (1) provides a very powerful tool and a way to avoid all computational difficulties associated with modeling of the unsteady flow field. In the case of simple longitudinal oscillations in a chamber of constant cross section, the functions in the summation are, for example:

$$\begin{cases} A_m(t) = \left(\frac{8n}{4n^2 + 1} \right) \sin\left(\frac{n\pi\bar{a}}{L}\right) \\ \psi_m(r) = \cos\left(\frac{n\pi z}{L}\right) \end{cases} \quad (2)$$

where L is the chamber length and z is the axial position. If Eq. (1) is evaluated with these parameters, then the waveform illustrated in Fig. 4(a) results. This should be compared to measured waveforms shown in Figs. 1(b) and 4(b). Although the individual components are effectively *standing* acoustic modes, the composite wave is a *traveling* steep fronted wave. Thus, one can accurately represent a traveling shock wave by superposition of standing acoustic waves. This is a powerful computational simplification.

G. Notation

The following dimensionless variables will be used (star * denotes dimensional quantities; subscript 0 indicates quiescent chamber reference conditions):

$$\begin{cases} p = p^*/P_0 \\ \rho = \rho^*/\rho_0 \\ T = T^*/T_0 \\ u = u^*/a_0 \\ r = r^*/L \end{cases} \quad \begin{cases} F = F^*/(\rho_0 a_0^2/L) \\ t = t^*/(L/a_0) \\ \omega = \omega^*/(a_0/L) \\ e = e^*/a_0^2 \end{cases} \quad (3)$$

where F is a body force and e is specific internal energy. The dimensionless governing equations are:

Continuity:

$$\frac{\partial \rho}{\partial t} + \nabla \cdot (\rho u) = 0 \quad (4)$$

Momentum:

$$\begin{aligned} \rho \left(\frac{\partial u}{\partial t} + \frac{1}{2} \nabla u \cdot u - u \times \omega \right) \\ = -\frac{1}{\gamma} \nabla p - \delta^2 \nabla \times \nabla \times u + \delta_a^2 \nabla (\nabla \cdot u) + F \end{aligned} \quad (5)$$

Energy:

$$\begin{aligned} \frac{\partial}{\partial t} \left[\rho \left(e + \frac{1}{2} u \cdot u \right) \right] + \nabla \cdot \left[\rho u \left(e + \frac{1}{2} u \cdot u \right) \right] \\ = \frac{\delta^2}{(\gamma - 1) Pr} \nabla^2 T - \frac{1}{\gamma} \nabla \cdot (\rho u) + \rho u \cdot (u \times \omega) \end{aligned}$$

$$\begin{aligned}
& +\mathbf{u} \cdot \mathbf{F} + \delta^2 [\boldsymbol{\omega} \cdot \boldsymbol{\omega} - \mathbf{u} \cdot \nabla \times \boldsymbol{\omega}] \\
& = +\delta_d^2 [(\nabla \cdot \mathbf{u})^2 + \mathbf{u} \cdot \nabla (\nabla \cdot \mathbf{u})] - \sum_{i=1}^N h_i^0 w_i
\end{aligned} \quad (6)$$

Species mass fraction:

$$\rho \left[\frac{\partial Y_i}{\partial t} + \mathbf{u} \cdot \nabla Y_i \right] - \frac{\delta^2}{Pr} \nabla^2 Y_i = w_i \quad (7)$$

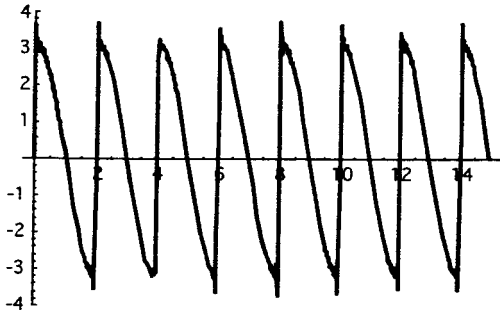
State:

$$p = \rho T \quad (8)$$

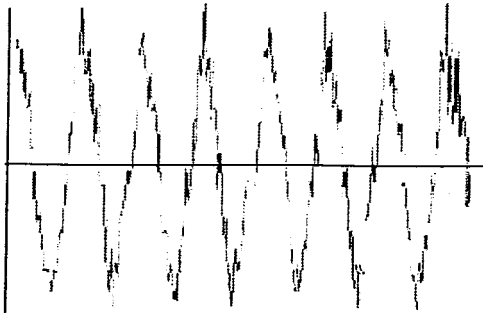
The Prandtl number Pr and viscous reference lengths (proportional to inverse square root of appropriate Reynolds numbers) appear naturally. These are defined as:

$$\begin{cases}
Pr \equiv \frac{c_p \mu}{\kappa} \\
\delta^2 = \frac{\nu}{a_0 L} \\
\delta_d^2 = \delta^2 \left(\eta / \mu + \frac{4}{3} \right) \\
\delta_f \equiv \frac{\kappa}{\rho_0 c_p V_{ref}} = \frac{\kappa}{\rho_0 c_p a_0 M_{ref}}
\end{cases} \quad (9)$$

The latter dimensionless length is the reference flame length needed in regions dominated by combustion heat release. Other variables needed in modeling chemical reactions are:



a) Waveform calculated via Eq. (1) using 20 modes



b) Preburner waveform during severe oscillation

Fig. 4 Measured versus calculated wave form.

$$\begin{cases}
w = w^* / (\rho_0 a_0 / L); & \text{reaction rate} \\
h_i^0 = h_i^{0*} / a_0^2; & \text{heat of combustion} \\
Y_i; & \text{mass fraction for species } i
\end{cases} \quad (10)$$

H. Separating Steady and Unsteady Parts

The steady and unsteady parts of the variables are decomposed in the standard manner by writing

$$\begin{cases}
\rho = \bar{\rho} + \rho^{(1)} \\
p = \bar{p} + p^{(1)} \\
T = \bar{T} + T^{(1)} \\
\mathbf{u} = \bar{\mathbf{M}}_b \mathbf{U} + \mathbf{u}^{(1)} \\
\boldsymbol{\omega} = \bar{\mathbf{M}}_b \nabla \times \mathbf{U} + \nabla \times \mathbf{u}^{(1)} = \bar{\mathbf{M}}_b \boldsymbol{\Omega} + \boldsymbol{\omega}^{(1)}
\end{cases} \quad (11)$$

Since the energy balance is the key to understanding the system behavior, let us carefully work with it. In what follows, we will avoid the common simplifying assumptions such as the isentropic flow limitation. We will also carefully include heat transfer and viscosity so that, in effect, we are modeling a wave system composed of superimposed waves of compressibility, vorticity, and entropy.

Define the system energy density as

$$\mathcal{E} \equiv \rho \left(e + \frac{1}{2} \mathbf{u} \cdot \mathbf{u} \right) \quad (12)$$

Then, for a calorically perfect gas, the energy equation becomes

$$\begin{aligned}
\frac{\partial \mathcal{E}}{\partial t} = & -\nabla \cdot \left[\rho \mathbf{u} \left(\frac{T}{\gamma(\gamma-1)} + \frac{1}{2} \mathbf{u} \cdot \mathbf{u} \right) \right] \\
& + \left\{ \begin{aligned}
& -\frac{1}{\gamma} \nabla \cdot (\rho \mathbf{u}) + \rho \mathbf{u} \cdot (\mathbf{u} \times \boldsymbol{\omega}) \\
& + \delta^2 [\boldsymbol{\omega} \cdot \boldsymbol{\omega} - \mathbf{u} \cdot \nabla \times \boldsymbol{\omega}] + \frac{\delta^2}{(\gamma-1)Pr} \nabla^2 T \\
& + \delta_d^2 [(\nabla \cdot \mathbf{u})^2 + \mathbf{u} \cdot \nabla (\nabla \cdot \mathbf{u})] + \dot{Q} + \mathbf{u} \cdot \mathbf{F}
\end{aligned} \right\} \quad (13)
\end{aligned}$$

where shorthand notation has been adopted for the distributed heat release in the combustion processes. The body force, \mathbf{F} , is a placeholder for several two-phase flow effects such as spray atomization, etc. that will be treated later. Note that the compressive viscous force and conduction heat transfer terms are retained. These are the source of the important nonlinear energy loss in steep wave fronts.

Using Eqs. (11), one can now expand Eq. (12) to give the equation for the system amplitude. To accomplish this, the time averaged Eq. (13) can be written as

$$2\epsilon \frac{d\epsilon}{dt} \langle \mathcal{E}_2 \rangle = \left\langle \begin{aligned} & -\nabla \cdot \left[\rho u \left(\frac{T}{\gamma(\gamma-1)} + \frac{1}{2} u \cdot u \right) \right] \\ & -\frac{1}{\gamma} \nabla \cdot (\rho u) + \rho u \cdot (u \times \omega) + u \cdot F + \dot{Q} \\ & + \delta^2 [\omega \cdot \omega - u \cdot \nabla \times \omega] + \delta_d^2 u \cdot \nabla (\nabla \cdot u) \\ & + \left\{ \frac{\delta^2}{(\gamma-1)Pr} \nabla^2 T + \delta_d^2 (\nabla \cdot u)^2 \right\} \end{aligned} \right\rangle \quad (14)$$

where

$$\langle \mathcal{E}_2 \rangle = \frac{1}{\gamma \bar{P}} \left\langle \left(\frac{p'}{\gamma} \right)^2 \right\rangle + \frac{1}{2} \bar{\rho} \langle u' \cdot u' \rangle \quad (15)$$

is the time averaged oscillatory energy. Note that this consists of a "potential" energy proportional to the pressure fluctuation and a kinetic part proportional to the square of the particle velocity. The latter is not the simple acoustic particle velocity; it is the composite of the irrotational and rotational parts needed to satisfy correct boundary conditions at the chamber surfaces.

Equation (15) is similar to the usual Kirchhoff reference energy density from classical acoustics:⁵⁴

$$\mathcal{E}_{\text{Kirchhoff}} = \frac{1}{2} \left[\frac{p^{(1)}}{\gamma} \right]^2 + \frac{1}{2} \bar{\rho} u^{(1)} \cdot u^{(1)} \quad (16)$$

The differences are the result of relaxing the isentropic flow assumption that was used in deriving Eq. (16).

I. Spatial Averaging

In order to account for the net behavior of the entire system it is now required to integrate the time-averaged energy density over the chamber control volume. Define the reference system energy,

$$E^2 \equiv \iiint_V \langle \mathcal{E}_2 \rangle dV = \iiint_V \left\langle \frac{1}{\gamma \bar{P}} \left(\frac{p'}{\gamma} \right)^2 + \frac{1}{2} \bar{\rho} u' \cdot u' \right\rangle dV \quad (17)$$

then the rate of change of system amplitude can be written in the convenient form:

$$\frac{d\epsilon}{dt} = \alpha^{(1)} \epsilon + \alpha^{(2)} \epsilon^2 + \alpha^{(3)} \epsilon^3 + \dots \quad (18)$$

where $\alpha^{(1)}$ is the linear growth rate for the composite wave system. This expression emphasizes the important fact that the nonlinear model is only as good as the linear representation of the system.

J. Linear Growth Rate

The linear part of Eq. (18) becomes

$$\alpha^{(1)} = \frac{1}{2E^2} \left\{ -\bar{M}_b \bar{P} \iint_S n \cdot \left\langle \frac{1}{2} U (u' \cdot u') + u' (U \cdot u') \right\rangle dS \right.$$

$$\begin{aligned} & -\frac{1}{\gamma} \iint_S n \cdot \langle p' u' \rangle dS - \frac{\bar{M}_b}{\gamma \bar{P}} \iint_S n \cdot U \langle (p'/\gamma)^2 \rangle dS \\ & + \bar{M}_b \bar{P} \iiint_V \langle u' \cdot (u' \times \omega) \rangle dV + \bar{M}_b \bar{P} \iiint_V U \cdot \langle u' \times \omega' \rangle dV \\ & + \delta^2 \iint_S n \cdot \langle u' \times \omega' \rangle dS + \delta_d^2 \iiint_V \langle u' \cdot \nabla (\nabla \cdot u') \rangle dV \\ & \left. + \iiint_V \langle \dot{Q} \rangle dV + \iiint_V \langle F \rangle dV \right\} \quad (19) \end{aligned}$$

where only the placeholders for combustion heat release and two-phase flow interactions are shown. It happens that careful evaluation of the volume integrals in Eq. (19) leads to cancellation of many of the terms.

In many ways, achieving a valid linear model is the most difficult part of the entire problem. It has in fact been the downfall of numerous past attempts. Much time and energy has been expended on attempts to correct deficiencies in the linear model by introduction of *ad hoc* fixes that are often based on guesswork, and misinterpretation and/or distortion of experimental evidence. The roadway is strewn with the wreckage of such attempts; we avoid the temptation to dwell on this unhappy aspect of the past. Clearly, the only path to success is to retain and carefully evaluate all of the physical information that has been so carefully collected in the system energy balance constructed here.

To illustrate the benefits of a complete energy balance as compared to earlier models based on the perturbed wave equation approach, we briefly examine the origins of the Culick *flow turning* effect. Flow turning has been a source of considerable debate, disagreement, and unhappiness in the solid propellant rocket instability research community. It introduces a major energy sink in stability assessments using the SSP (standard stability prediction) algorithm. Unfortunately, this term leads to a damping effect which in most motor evaluations is as large as other main contributions to the energy balance including the combustion-related pressure coupling effects. We now demonstrate the handling of terms in Eq. (19), to evaluate the term from which flow turning originates, namely:

$$\alpha_4^{(1)} = \frac{\bar{M}_b \bar{P}}{2E^2} \iiint_V (U \cdot \langle u' \times \omega' \rangle + \langle u' \cdot U \times \omega' \rangle) dV \quad (20)$$

The subscript, 4, is an artifact of a numbering system introduced in Ref. (11) to keep track of the many linear stability contributions in Eq. (19). Flow turning was first identified by Culick^{23,55} in his one-dimensional calculations. It appeared as a result of forcing satisfaction the no-slip condition (which could not be accomplished in his three-dimensional model because

of the irrotational flow assumption). Flandro^{17,18,26,56} later showed that the actual source of the flow turning was the irrotational part of the second term in Eq. (20). No earlier stability calculations incorporate the full set of rotational terms included in Eq. (20). When *all* of the terms are properly accounted for, and by applying the standard scalar triple product identity

$$\mathbf{A} \cdot (\mathbf{B} \times \mathbf{C}) = \mathbf{B} \cdot (\mathbf{C} \times \mathbf{A})$$

we discover that

$$\begin{aligned} \mathbf{U} \cdot \langle \mathbf{u}' \times \boldsymbol{\omega}' \rangle + \langle \mathbf{u}' \cdot \mathbf{U} \times \boldsymbol{\omega}' \rangle \\ = \langle -\mathbf{u}' \cdot \mathbf{U} \times \boldsymbol{\omega}' \rangle + \langle \mathbf{u}' \cdot \mathbf{U} \times \boldsymbol{\omega}' \rangle = 0 \end{aligned} \quad (21)$$

Flow turning has now completely vanished; a result that agrees with experimental evidence and with other independently conducted analyses.^{57,58}

This correction alone leads to major improvement in agreement with experimental data. The lesson here is that only by accounting for *all* unsteady energy gains and losses can a correct linear stability theory be achieved. Other terms in Eq. (19) once thought to have important stability implications do not appear when the integrals are carefully evaluated.

We have recently completed a full evaluation of Eq. (19) for the solid motor case;^{10,11} current efforts are focused on a similar evaluation for the liquid motor case.⁵⁹ A major effort is now being devoted to the important transverse mode case of central importance in large liquid engine development programs.⁵⁹

K. Linear Driving Mechanisms

Equation (19) clearly shows all potentially important sources of unsteady energy as well as damping effects. Many years of experience have shown that the first pair of terms represented by the surface integral

$$\alpha_1^{(1)} = -\frac{1}{2\gamma E^2} \iint_S \left(\langle p' \mathbf{n} \cdot \hat{\mathbf{u}} \rangle + \frac{\bar{M}_b}{\gamma^2 \bar{P}} \mathbf{n} \cdot \mathbf{U} \langle p'^2 \rangle \right) dS \quad (22)$$

play a major role in driving waves. It is also the origin of the important nozzle damping effect. In cases where the combustion energy release occurs close to the surface (as in a burning solid propellant) or near the injector surface, this term is the primary source of unsteady energy. At first glance, it appears that Eq. (22) should represent zero contribution since for acoustic motions the pressure and velocity fluctuations are 90° out of phase. However, one must account for the phase shift in the combustion zone region of nonuniformity. This is done in the solid propellant case by introducing the admittance function accounting for myriad chemical and physical processes within the flame zone. For example, one defines

$$\mathbf{n} \cdot \hat{\mathbf{u}} = -\bar{M}_b A_b^{(r)} \frac{p'}{\gamma} \quad (23)$$

expressing the normal velocity fluctuation in terms of the pressure disturbance that creates it. Major effort is expended in the solid rocket community in characterizing the admittance function.

This is a familiar scenario and need not be treated in depth here. The solid rocket literature is replete with discussion of this important concept. A lucid treatment can be found in Ref. 26. The associated nozzle damping is also described in detail in this and many other documents. The nozzle damping plays an important role in the preburner oscillations.

The first term in Eq. (22) is also a potent source of energy in the preburner problem. If $\langle p' \mathbf{n} \cdot \hat{\mathbf{u}} \rangle$ is evaluated at the injection surface accounting for the phase difference between fluctuations in the incoming oxidizer and fuel particle velocities and the pressure oscillations at the interface, it will be seen that a powerful analog to the solid rocket pressure coupling is identified. This is related to the well-known "injector coupling" mechanism. However, it allows a quantitative estimate of this driving effect. Examination of the preburner experimental data shows that indeed the pressures in the LOX and H₂ feed lines upstream of the injector reflect the pressure fluctuations in the chamber and exhibit the phase differences needed to explain this powerful unsteady energy source. Additional energy is supplied to the waves via the more traditional distributed combustion; this is enhanced by the phase shifts already present in the injectants as they enter the combustion zone. However, there can be no doubt that any energy source located near a pressure antinode (*e.g.* at the injector surface) is a potent driver of oscillations of the type observed. These matters are currently undergoing thorough study by the authors and their coworkers, and we expect that they will play a major role in the predictive algorithm under development by our research group.

L. Effects of Nonlinearity

It is now required to examine nonlinear terms arising from the expansion of Eq. (14). The most important of these are the energy losses incurred in steep wave fronts. Let us focus on the last set of terms in Eq. (14). After temporal and spatial averaging, we are left with

$$\iiint_V \left\langle \frac{\delta^2}{(\gamma-1)Pr} \nabla^2 T + \delta_d^2 (\nabla \cdot \mathbf{u})^2 \right\rangle dV \quad (24)$$

Those readers experienced in gasdynamics will recognize in this term the source of the entropy gain and associated energy loss in a steep wave front. In

fact, this term is usually ignored because it is only important if there are very steep gradients in particle velocity and temperature. Let us evaluate this term by considering a very small portion of the chamber volume that encompasses the shock layer formed by a steepened wave system as described earlier. The shock layer can be treated as a region of nonuniformity as illustrated in Fig. 5.

Following standard procedures Eq. (23) can be reduced to the classical textbook result showing the origin of the entropy gain in the shockwave. By manipulations using the Rankine-Hugoniot equations, we find the formula for the energy loss in the steep wave to be

$$\left(\frac{dE}{dt}\right)_{\text{shock}} = -\frac{S_{\text{port}} (s_2 - s_1)^*}{\gamma(\gamma-1) c_v} = -\left(\frac{\epsilon_{\text{shock}}}{\bar{P}}\right)^3 S_{\text{port}} \left(\frac{\gamma+1}{12\gamma^3}\right) \quad (25)$$

leading to a simple approximation for the nonlinear stability parameter in Eq. (18), namely

$$\alpha^{(2)} = -\frac{(\gamma+1)}{3E^2} \left(\frac{\xi}{2\gamma}\right)^3 S_{\text{port}} \quad (26)$$

where ξ is a factor (of order 1), which is dependent upon the waveform used to represent for the traveling

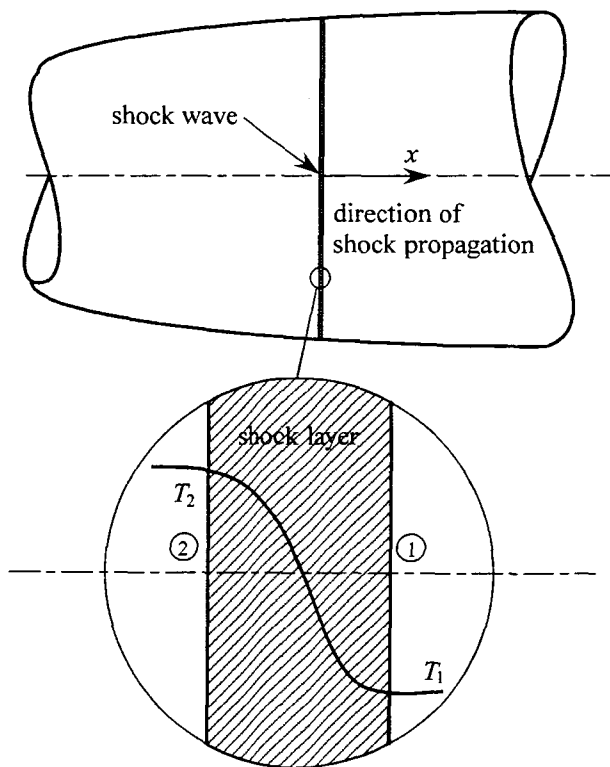


Fig. 5 Shock layer structure.

shock wave. S_{port} is the area of the shock front. In the longitudinal case, this is simply the cross-sectional area of the duct at a convenient location; the forward chamber area is a good choice.

This nonlinear loss effect is the principal damping mechanism in both liquid engines and solid propellant motors, and is the key element in understanding the limit cycle behavior so often encountered when finite amplitude waves appear.

It is tempting to carry the implied perturbation series in Eq. (18) to higher than second order in the system amplitude. However, this is not justified in the present situation because we assume that the unsteady flow field and mode shape information for the chamber is accurate only to the first order in wave amplitude. Let us now test the results that we have found against experimental evidence.

M. Limit Cycle Amplitude

In liquid propellant engines one is seldom interested in tracing the details of the growth of the waves to their final state. Such engines usually operate for very long time (measured on the time scale of the wave motions) with correspondingly slow changes in the steady operating parameters. For this reason, strictly linear models provide very little useful information in the predictive sense. There is, however, a well-known rule of thumb that suggests that large values of the linear growth rate, $\alpha^{(1)}$, estimated for example by using Eq. (19) correlate with large values of the limit cycle amplitude. Clearly it is the latter amplitude that is of concern from the engine design point of view, since it is a measure of the vibration and other impacts on the system integrity due to the oscillations.

What is required is knowledge of the limit amplitude reached as the wave system approaches a fully steepened form. Equation (18) provides the required formula for the limit amplitude. In the fully steepened state, the wave amplitude is stationary, and it is readily seen that the limit amplitude is

$$\epsilon_{\text{limit}} = -\frac{\alpha^{(1)}}{\alpha^{(2)}}, \quad (27)$$

a physically meaningful only when $\alpha^{(2)}$ is negative. This will always be the case for the shock loss mechanism described by Eq. (24) since it is the outcome of a positive definite entropy gain. This expression has been tested for many solid rocket data sets and has been found to yield an excellent estimate of the limit amplitude. Again, please note that good results depend critically on a valid linear stability estimate.

N. Triggering Amplitude

This is a controversial subject. If one examines Fig. 5, in the context of Eq. (18) including terms to higher orders in the wave amplitude (fourth-order is required), it is theoretically possible to raise the amplitude of a system oscillating at its lowest limit amplitude to a yet higher limit amplitude by hard pulsing. That is, if the system receives sufficient energy to raise the oscillations above the critical triggering level as described in the figure, it may transition to a higher limit amplitude. This is what might be termed *true triggering*.

Careful examination of solid rocket data shows that this scenario seldom fits what is actually observed. In every case studied by the authors, motors that have exhibited "triggering" were actually linearly unstable motors. That is, they are not stable motors that are *triggered* into a high-amplitude limit cycle. When such motors operate without deliberate pulsing, the wave system grows so slowly from the random noise that oscillations may be barely measurable by the end of the burn.

However, when the motor receives a hard pulse, the broadband energy increment almost instantaneously excites finite amplitude steep fronted waves. Clearly, as Eq. (18) shows, the time to reach the limit cycle depends on the initial system ε created in the pulse. The system then either grows rapidly to its limit cycle amplitude or it may decay to the limit amplitude if the pulse starts the motion at ε higher than the limit amplitude. Calculations using Eq. (27) agree very well with actual observations.

We believe that true triggering is seldom, if ever, observed in practice. Much of the confusion over this issue has resulted from application of faulty predictive codes that almost always predict a linearly stable system. A classic example can be found in the recent experiments by Blomshield.¹ All motors fired in this test series were predicted by the SSP algorithm to be linearly stable. In fact, most of the motors were linearly *unstable* at least during part of the burn. Unless excited by a sufficiently hard pulse, only very low-level oscillations were present. Strong pulsing during otherwise leisurely (linearly unstable) operation led to violent oscillations in many tests.

O. The Mean Pressure Excursion

The preburner data, Fig. 2, clearly show a rise in mean chamber pressure accompanying high-amplitude longitudinal mode oscillations. A test of the validity of the theory presented in this paper is its ability to predict this important classical feature of combustion instability. What we will demonstrate here is that the same mechanism that drives the oscillations (first term

in Eq. (22)) is also the source of the DC shift phenomenon. This is a new result that has been shown to agree very well with experimental data in the solid motor case.^{1,10,11} Until now, explaining the mean pressure excursion required invocation of *ad hoc* "velocity coupling" effects or "acoustic erosivity".⁵¹ These confusing and misleading paraphernalia can now be discarded.

The source of the DC shift is readily found if nonlinear terms are retained in the continuity equation. Expanding Eq. (3) and taking the time average yields

$$\frac{d\bar{P}}{dt} = -\nabla \cdot (\bar{M}_b \bar{\rho} U) - \frac{1}{\gamma} \nabla \cdot \langle p^{(1)} u^{(1)} \rangle \quad (28)$$

where the first term on the right represents the usual quasi-steady mass flux at the chamber boundaries. The similarity of the second term to the pressure coupled acoustic driving in Eq. (22) is obvious. Integration over the chamber volume leads to the formula for the rate of change of the quasi-steady chamber operating pressure:

$$\frac{d\bar{P}}{dt} = - \left\{ \begin{aligned} &\frac{1}{V} \iint_S \mathbf{n} \cdot (\bar{\rho} \bar{M}_b U) dS \\ &+ \frac{1}{\gamma V} \iint_S \mathbf{n} \cdot \langle p^{(1)} u^{(1)} \rangle dS \end{aligned} \right\} \quad (29)$$

The first term is handled by means of standard steady internal ballistics calculations. The second leads to the mean pressure shift. Notice that it is proportional to the second order of the wave amplitude. Equation (29) establishes the intimate coupling between the pressure rise and the growth and limiting of the pressure oscillations.

P. Simulating and Predicting Preburner Behavior

The results for the nonlinear system growth and the corresponding mean pressure excursion must be computed simultaneously. When the several system models are evaluated and the integrals are performed, we are left with a pair of coupled nonlinear, ordinary differential equations:

$$\begin{cases} \frac{d\varepsilon}{dt} = \alpha^{(1)} \varepsilon + \alpha^{(2)} \varepsilon^2 + \dots \\ \frac{d\bar{P}}{dt} = \beta^{(1)} + \beta^{(2)} \varepsilon^2 \end{cases} \quad (30)$$

These are readily solved using a simple numerical algorithm. The result is the time history of the growth and limiting of the pressure oscillation amplitude and the accompanying growth and limiting of the mean pressure amplitude. These results agree in every way with the preburner instability data set.

IV. Conclusions

It is not possible at the present time to display results comparing the preburner experimental data with predictions from the algorithm just described. Much remains to be accomplished in carrying out the details. A computer algorithm is being written to enable the motor analyst/designer to predict the stability of a given system and to diagnose sets of experimental data.

In order to aid the reader in envisioning the possibilities, we show here some recent results from a similar application of Eq. (30) in a difficult solid rocket instability problem. In many ways, the instability experienced in this example case closely parallels what has been observed in the liquid propellant preburner situation.

A set of tactical solid motors of varying geometry and propellant characteristics were tested by Dr. F. Blomshield at NAWC, China Lake, CA.^{1,60-64} In virtually all cases the standard stability prediction code (SPP) predicted stable behavior. Yet, many of the motors were readily pulsed into violent oscillations. Fig. 6 shows a pressure vs. time trace for a cylindrical motor from this test series. The progressive pressure rise results from the increasing burning surface area with time. The mean pressure shift and pressure oscillations are clearly shown. Data came from a pressure transducer at the motor forward end. As in the case of the preburner data depicted in Fig. 2, this motor exhibited a spectrum dominated by the 1L (first longitudinal mode) accompanied by a great many harmonics – strong evidence for steep-fronted waves as already described.

Figure 7 shows the predicted behavior for this motor found by solving Eq. (30) using only geometrical and physical data from the tests – no curve fitting was employed. All important features of the actual data are well represented. Note that even though the system is linearly unstable, no wave growth or DC shift occurs unless the motor is pulsed.

To summarize: we have devised a new procedure for estimating the tendency for a given rocket motor chamber to exhibit nonlinear combustion instability. The new algorithm gives not only growth rate information and the associated stability maps, but more importantly predicts the evolution of the system oscillation amplitude and the mean pressure shift. These analytical/numerical tools promise to give the motor designer the ability to avoid design features that may promote combustion instability much earlier in the development cycle than possible using other methods.

If combustion instability problems are encountered in the test phase of engine development, these new tools yield an improved method for correlating experimental

data and for correctly interpreting the results. They also provide the ability to test and perfect corrective mechanisms if these become necessary.

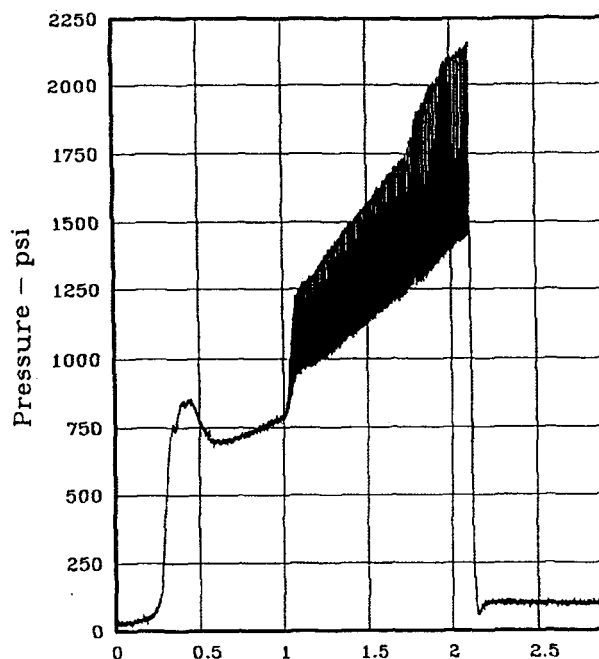


Fig. 6 Pressure vs. time for motor No. 9.¹

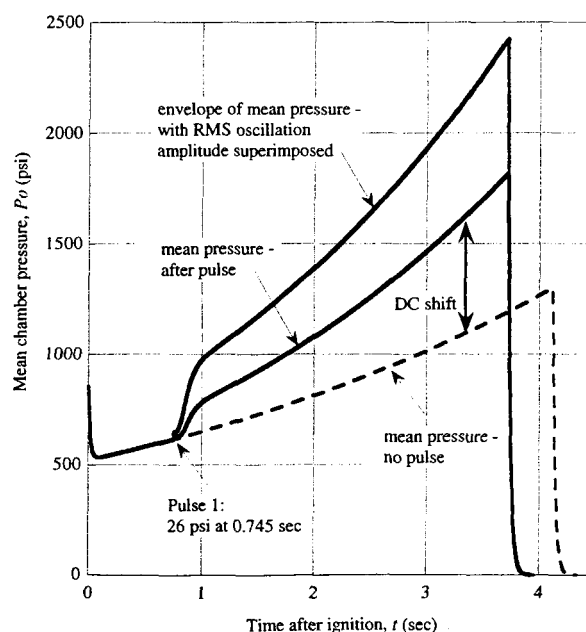


Fig. 7 Simulation of motor No. 9.^{10,11}

Acknowledgments

This work was sponsored partly by the University of Tennessee, UTSI, and partly by the NASA Marshall Spaceflight Center, under Grant No. NNM04AA30G, Technical Officer, J. D. Sims. The first author wishes to express appreciation for additional support from the Edward J. and Carolyn P. Boling Chair of Excellence in Advanced Propulsion, University of Tennessee.

References

- ¹Blomshield, F. S., "Stability Testing and Pulsing of Full Scale Tactical Motors, Parts I and II," Naval Air Warfare Center, NAWCWPNS TP 8060, February 1996.
- ²Boys, S. F. a. S., A., "Studies Accessory to the Development of Classified Rockets," Woolwich Arsenal, England, 1942.
- ³Brownlee, W. G., "An Experimental Investigation of Unstable Combustion in Solid Propellant Rocket Motors," Ph.D. Dissertation, California Institute of Technology, 1959.
- ⁴Levine, J. N., and Baum, J. D., "A Numerical Study of Nonlinear Phenomena in Solid Rocket Motors," *AIAA Journal*, Vol. 21, No. 4, 1983, pp. 557-564.
- ⁵Brownlee, W. G., "Nonlinear Axial Combustion Instability in Solid Propellant Motors," *AIAA Journal*, Vol. 2, No. 2, 1964, pp. 275-284.
- ⁶Flandro, G. A., "Approximate Analysis of Nonlinear Instability with Shock Waves," AIAA Paper 82-1220, July 1982.
- ⁷Flandro, G. A., "Energy Balance Analysis of Nonlinear Combustion Instability," *Journal of Propulsion and Power*, Vol. 1, No. 3, 1985, pp. 210-221.
- ⁸Flandro, G. A., "Analysis of Nonlinear Combustion Instability," SIAM Minisymposium, March 1998.
- ⁹Green, J., L., "Observations on the Irregular Reaction of Solid Propellant Charges," *Jet Propulsion*, Vol. 26, 1956, pp. 655-659.
- ¹⁰Flandro, G. A., Majdalani, J., and French, J. C., "Nonlinear Rocket Motor Stability Prediction: Limit Amplitude, Triggering, and Mean Pressure Shift," AIAA Paper 2004-4054, July 2004.
- ¹¹Flandro, G. A., Majdalani, J., and French, J. C., "Incorporation of Nonlinear Capabilities in the Standard Stability Prediction Program," AIAA Paper 2004-4182, July 2004.
- ¹²Sotter, J. G., Woodward, J. W., and Clayton, R. M., "Injector Response to Strong High-Frequency Pressure Oscillations," *Journal of Spacecraft and Rockets*, Vol. 6, No. 4, 1969, pp. 504-506.
- ¹³Sotter, J. G., and Clayton, R. M., "Monitoring the Combustion Process in Large Engines," *Journal of Spacecraft and Rockets*, Vol. 4, No. 5, 1967, pp. 702-703.
- ¹⁴Clayton, R. M., "Experimental Measurements on Totating Detonation-Like Combustion," JPL, Technical Rept. 32-788, Pasadena, CA, August 1965.
- ¹⁵Clayton, R. M., Rogero, R. S., and Sotter, J. G., "An Experimental Description of Destructive Liquid Rocket Resonant Combustion," *AIAA Journal*, Vol. 6, No. 7, 1968, pp. 1252-1259.
- ¹⁶Flandro, G. A., "Nonlinear Unsteady Solid Propellant Flame Zone Analysis," AIAA Paper 98-3700, 1998.
- ¹⁷Flandro, G. A., "Effects of Vorticity on Rocket Combustion Stability," *Journal of Propulsion and Power*, Vol. 11, No. 4, 1995, pp. 607-625.
- ¹⁸Flandro, G. A., and Majdalani, J., "Aeroacoustic Instability in Rockets," *AIAA Journal*, Vol. 41, No. 3, 2003, pp. 485-497.
- ¹⁹Culick, F. E. C., and Yang, V., "Overview of Combustion Instabilities in Liquid Propellant Rocket Engines," *Liquid Rocket Engine Combustion Instability*, Vol. 169, edited by V. Yang and W. E. Anderson, AIAA Progress in Astronautics and Aeronautics, 1995, pp. 1-37.
- ²⁰Culick, F. E. C., "Combustion Instabilities in Propulsion Systems," *Unsteady Combustion*, Kluwer Academic Publishers, 1996, pp. 173-241.
- ²¹Culick, F. E. C., "A Note on Rayleigh's Criterion," *Combustion Science and Technology*, Vol. 56, 1987, pp. 159-166.
- ²²Culick, F. E. C., "Stability of Three-Dimensional Motions in a Rocket Motor," *Combustion Science and Technology*, Vol. 10, No. 3, 1974, pp. 109-124.
- ²³Culick, F. E. C., "The Stability of One-Dimensional Motions in a Rocket Motor," *Combustion Science and Technology*, Vol. 7, No. 4, 1973, pp. 165-175.
- ²⁴Culick, F. E. C., "High Frequency Oscillations in Liquid Rockets," *AIAA Journal*, Vol. 1, No. 5, 1963, pp. 1097-1104.
- ²⁵Culick, F. E. C., and Yang, V., "Prediction of the Stability of Unsteady Motions in Solid Propellant Rocket Motors," *Nonsteady Burning and Combustion Stability of Solid Propellants*, Vol. 143, edited by L. De Luca, E. W. Price, and M. Summerfield, AIAA Progress in Astronautics and Aeronautics, Washington, DC, 1992, pp. 719-779.
- ²⁶Flandro, G. A., "On Flow Turning," AIAA Paper 95-2530, July 1995.
- ²⁷Flandro, G. A., Cai, W., and Yang, V., "Turbulent Transport in Rocket Motor Unsteady Flowfield," *Solid*

Propellant Chemistry, Combustion, and Motor Interior Ballistics, Vol. 185, edited by V. Yang, T. B. Brill, and W.-Z. Ren, AIAA Progress in Astronautics and Aeronautics, Washington, DC, 2000, pp. 837-858.

²⁸Majdalani, J., Flandro, G. A., and Roh, T. S., "Convergence of Two Flowfield Models Predicting a Destabilizing Agent in Rocket Combustion," *Journal of Propulsion and Power*, Vol. 16, No. 3, 2000, pp. 492-497.

²⁹Majdalani, J., and Van Moorhem, W. K., "Improved Time-Dependent Flowfield Solution for Solid Rocket Motors," *AIAA Journal*, Vol. 36, No. 2, 1998, pp. 241-248.

³⁰Majdalani, J., "The Boundary Layer Structure in Cylindrical Rocket Motors," *AIAA Journal*, Vol. 37, No. 4, 1999, pp. 505-508.

³¹Majdalani, J., "Vorticity Dynamics in Isobarically Closed Porous Channels. Part I: Standard Perturbations," *Journal of Propulsion and Power*, Vol. 17, No. 2, 2001, pp. 355-362.

³²Majdalani, J., and Roh, T. S., "Vorticity Dynamics in Isobarically Closed Porous Channels. Part II: Space-Reductive Perturbations," *Journal of Propulsion and Power*, Vol. 17, No. 2, 2001, pp. 363-370.

³³Majdalani, J., and Roh, T. S., "The Oscillatory Channel Flow with Large Wall Injection," *Proceedings of the Royal Society, Series A*, Vol. 456, No. 1999, 2000, pp. 1625-1657.

³⁴Vuillot, F., and Avalon, G., "Acoustic Boundary Layer in Large Solid Propellant Rocket Motors Using Navier-Stokes Equations," *Journal of Propulsion and Power*, Vol. 7, No. 2, 1991, pp. 231-239.

³⁵Roh, T. S., Tseng, I. S., and Yang, V., "Effects of Acoustic Oscillations on Flame Dynamics of Homogeneous Propellants in Rocket Motors," *Journal of Propulsion and Power*, Vol. 11, No. 4, 1995, pp. 640-650.

³⁶Yang, V., and Roh, T. S., "Transient Combustion Response of Solid Propellant to Acoustic Disturbance in Rocket Motors," AIAA Paper 95-0602, January 1995.

³⁷Vuillot, F., "Numerical Computation of Acoustic Boundary Layers in Large Solid Propellant Space Booster," AIAA Paper 91-0206, January 1991.

³⁸Baum, J. D., Levine, J. N., and Lovine, R. L., "Pulsed Instabilities in Rocket Motors: A Comparison between Predictions and Experiments," *Journal of Propulsion and Power*, Vol. 4, No. 4, 1988, pp. 308-316.

³⁹Baum, J. D., "Investigation of Flow Turning Phenomenon; Effects of Frequency and Blowing Rate," AIAA Paper 89-0297, January 1989.

⁴⁰Glick, R. L., and Renie, J. P., "On the Nonsteady Flowfield in Solid Rocket Motors," AIAA Paper 84-1475, June 1984.

⁴¹Brown, R. S., Blackner, A. M., Willoughby, P. G., and Dunlap, R., "Coupling between Acoustic Velocity Oscillations and Solid Propellant Combustion," *Journal of Propulsion and Power*, Vol. 2, No. 5, 1986, pp. 428-437.

⁴²Shaeffer, C. W., and Brown, R. S., "Oscillatory Internal Flow Field Studies," United Technologies, AFOSR Contract Rept. F04620-90-C-0032, San Jose, CA, August 1990.

⁴³Shaeffer, C. W., and Brown, R. S., "Oscillatory Internal Flow Studies," United Technologies, Chemical Systems Div. Rept. 2060 FR, San Jose, CA, August 1992.

⁴⁴Cantrell, R. H., and Hart, R. W., "Interaction between Sound and Flow in Acoustic Cavities: Mass, Momentum, and Energy Considerations," *Journal of the Acoustical Society of America*, Vol. 36, No. 4, 1964, pp. 697-706.

⁴⁵Dawson, M. C., and Flandro, G. A., "Elimination of Flow Induced Instabilities in Solid Rocket Motors by Aerodynamic Contouring of Internal Grain Geometries," Air Force Rocket Propulsion Laboratory, AFRPL TR-82-058, January 1983.

⁴⁶Flandro, G. A., "Vortex Driving Mechanisms in Oscillatory Rocket Flows," *AIAA Journal of Propulsion and Power*, Vol. 2, No. 3, 1986, pp. 206-214.

⁴⁷Flandro, G. A. a. J., H. R., "Vortex Generated Sound in Cavities," *Aeroacoustics: Jet and Combustion Noise, Aiaa Progress Series in Aeronautics and Astronautics*, Vol. 37, MIT Press, 1975.

⁴⁸Saenger, R. A. a. H., G. E., "Periodic Shock Waves in Resonating Gas Columns," *Journal of the Acoustical Society of America*, Vol. 32, No. 8, 1960, pp. 961-970.

⁴⁹Chester, W., "Resonant Oscillations in Closed Tubes," *Journal of Fluid Mechanics*, Vol. 18, No. 1, 1964, pp. 44-64.

⁵⁰Harje, D. T., and Reardon, F. H., "Liquid Propellant Rocket Combustion Instability," NASA, Technical Rept. SP-194, July 1972.

⁵¹Levine, J. N. a. B., J. D., "A Numerical Study of Nonlinear Instability Phenomena in Solid Rocket Motors," *AIAA Journal*, Vol. 21, No. 4, 1983, pp. 557-564.

⁵²Sirignano, W. A. a. C., L., "A Shock Wave Model of Unstable Rocket Combustion," *AIAA Journal*, Vol. 2, No. 7, 1964.

⁵³Culick, F. E. C., "Non-Linear Growth and Limiting Amplitude of Acoustic Oscillations in Combustion Chambers," *Combustion Science and Technology*, Vol. 3, No. 1, 1971, pp. 1-16.

⁵⁴Kirchoff, G., *Vorlesungen Über Mathematische Physik: Mechanik*, 2nd ed., Teubner, Leibzig, 1877, pp. 311-336.

⁵⁵Culick, F. E. C., "Stability of Longitudinal Oscillations with Pressure and Velocity Coupling in a Solid Propellant Rocket," *Combustion Science and Technology*, Vol. 2, No. 4, 1970, pp. 179-201.

⁵⁶Flandro, G. A., and Roach, R. L., "Effects of Vorticity Production on Acoustic Waves in a Solid Propellant Rocket," Air Force Office of Scientific Research, AFOSR Final Rept. 2060 FR, Bolling AFB, DC, October 1992.

⁵⁷Malhotra, S., "On Combustion Instability in Solid Rocket Motors," Dissertation, California Institute of Technology, 2004.

⁵⁸Van Moorhem, W. K., "An Investigation of the Origin of the Flow Turning Effect in Combustion Instability," 17th JANNAF Combustion Conference, September 1980.

⁵⁹Flandro, G. A., Majdalani, J., and Sims, J. D., "Nonlinear Longitudinal Mode Instability in Liquid Propellant Rocket Engine Preburner," AIAA Paper 2004-4162, July 2004.

⁶⁰Blomshield, F. S., Mathes, H. B., Crump, J. E., Beiter, C. A., and Beckstead, M. W., "Nonlinear Stability Testing of Full-Scale Tactical Motors," *Journal of Propulsion and Power*, Vol. 13, No. 3, 1997, pp. 356-366.

⁶¹Blomshield, F. S., Bicker, C. J., and Stalnaker, R. A., "High Pressure Pulsed Motor Firing Combustion Instability Investigations," *Proceedings of the 1996 JANNAF 33rd Combustion Meeting*, Naval Postgraduate School, Monterey, CA, 1996.

⁶²Blomshield, F. S., Crump, J. E., Mathes, H. B., Stalnaker, R. A., and Beckstead, M. W., "Stability Testing of Full-Scale Tactical Motors," *Journal of Propulsion and Power*, Vol. 13, No. 3, 1997, pp. 349-355.

⁶³Blomshield, F. S., and Mathes, H. B., "Pressure Oscillations in Post-Challenger Space Shuttle Redesigned Solid Rocket Motors," *Journal of Propulsion and Power*, Vol. 9, No. 2, 1993, pp. 217-221.

⁶⁴Maslen, S. H., and Moore, F. K., "On Strong Transverse Waves without Shocks in a Circular cylinder," *Journal of the Aeronautical Sciences*, Vol. 23, 1956, pp. 583-593.